Acta Materialia 194 (2020) 276–282

Contents lists available at ScienceDirect

Acta Materialia

journal homepage: www.elsevier.com/locate/actamat

Full length article

# Mysterious failure in load-free superalloys under repeated thermal shocks

Junxia Wen[a,b,c], Rui Cao[a,b,*], Yanfei Gao[c,*]

[a] State Key Laboratory of Advanced Processing and Recycling of Nonferrous Metals, Lanzhou University of Technology, Lanzhou 730050, Gansu, China
[b] School of Materials Science and Engineering, Lanzhou University of Technology, Lanzhou 730050, Gansu, China
[c] Department of Materials Science and Engineering, University of Tennessee, Knoxville, TN 37996, USA

ARTICLE INFO

*Article History:*
Received 9 January 2020
Revised 22 March 2020
Accepted 1 May 2020
Available online 18 May 2020

*Keywords:*
Superalloy
Thermal fatigue
Concomitant oxidation-diffusion-creep processes
Stokes-Herring-Suo model
Preferential oxidation

ABSTRACT

The increase of heat engine efficiency is highly demanded in applications such as gas turbines and fossil-fired power plants, which has posed prime challenges and opportunities for the development of high temperature alloys under extreme creep-fatigue-oxidation conditions. Besides the widely investigated turbine blade alloys and their coatings, many other components could be load-free or nearly so, but fracture failure and preferential oxidation are nevertheless found when subjected to repeated thermal shocks. This work is based on a specific contrast of oxidation behavior in load-free Co-Cr-C-W superalloys under isothermal and cyclic thermal conditions. First, we establish a mechanistic model on the stress generation arising from concomitant oxidation-diffusion-creep processes, based on the Stokes-Herring-Suo formalism. Because chromium diffuses from the substrate to the oxide-alloy interface, the divergence of this uniaxial diffusion flux is non-trivial, so that the lateral creep deformation is invoked to satisfy the kinematic constraint. Second, the preference of the oxide scale or "fingers" is found to depend on the degree of the above oxidation stress. Under the conditions of long fingers (as compared to the chromium depletion zone) and low oxidation stresses (as compared to the oxide strength), these fingers will grow and penetrating into the substrate, and thus subsequently the material fracture resistance is degraded. The above two lines of thought provide a mechanistic interpretation of thermal fatigue failure without external load, and help the further design of alloys under extreme thermal, mechanical, and corrosive conditions.



## 1. Introduction

The ever-increasing demand of better materials during the jet age and the nuclear age in the past many decades has posed great challenges to the physical and mechanical metallurgy community [1,2]. Facing an even tougher goal of increasing the efficiency of heat engines, particularly for combating the climate change, a multitude of extreme conditions are becoming the norm for next-generation turbines and power generation systems, including, for examples, higher temperature for single crystalline superalloys [3], better performing thermal barrier coatings [4,5], improved resistance to creep-fatigue and stress corrosion cracking [6–10], degradation prevention in welded components [11,12], and the synergy of thermomechanical and oxidation processes [13–15], among many others. A fair understanding has been developed for high temperature failure under monotonic or few cycles of mechanical loads, but it remains elusive to model and predict the creep-fatigue-oxidation failure in typical realistic applications [6]. Despite a variety of microscopic investigations of oxidation and diffusional processes, e.g., [16,17], the primary hurdle for the creep-fatigue-oxidation study rather lies on the frequent confrontation of mysterious and previously unseen failure modes. One quintessential example along this line is the observation of low cycle fatigue in superalloys under compression-compression strain cycles but without thermal cycles[14,15]. The thermally grown oxide (TGO) will become localized and penetrate into the substrate superalloy, and this extension progresses cycle-by-cycle. This mysterious failure has been understood as the preference of TGO extending in depth direction over expanding/thickening laterally when TGO deforms elastically as opposed to plastically. The mechanical property mismatch between TGO and superalloy substrate, together with the compressive strain cycles, determines the deformation behavior in TGO.

This work deals with yet another mysterious failure in superalloys under oxidizing condition. As shown in Fig. 1(a), a long oxide "finger" is found to progressively extend in the depth direction of a Co-based superalloy, which is under no external load but with repeated thermal shocks as schematically illustrated therein [18–20]. When used away from the combustion chamber in heat engines, cemented

* Corresponding authors.
*E-mail addresses:* caorui@lut.edu.cn (R. Cao), ygao7@utk.edu (Y. Gao).

https://doi.org/10.1016/j.actamat.2020.05.002
1359-6454/

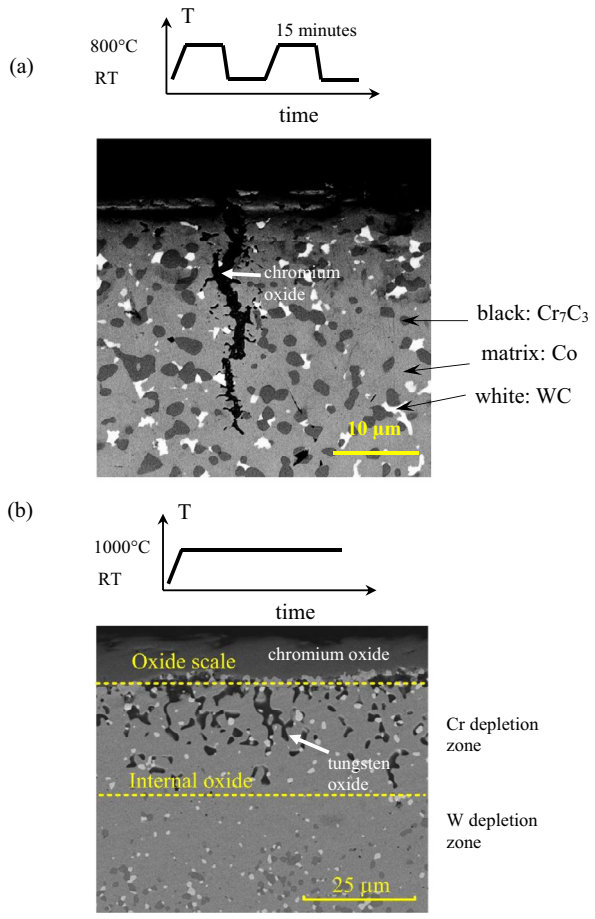


**Fig. 1.** Contrasting oxidation behavior in Stellite 12 (Co-29Cr-2.3C-3W) cobalt-based superalloy (experimental details can be found in [18-20]). In the scanning electron microscopy (SEM) images, the gray phase is the Co-based matrix, the white phase is WC, and the black phase is $Cr_7C_3$. (a) The formation of oxide "fingers" under repeated thermal shocks, with the temperature ranging from room temperature (RT) to 800 °C and with the hold period of 15 min. This image was taken after 30 thermal cycles. The energy-dispersive spectroscopy (EDS) analysis identifies these fingers as chromium oxide. (b) No chromium oxide fingers were found in isothermal oxidation condition (1000 °C after 200 h for this image). Earthworm-like phases are identified as tungsten oxide from EDS analysis, as also confirmed from the related Cr-depleted and W-depleted zones.

carbines embedded in the Co-based matrix provide the needed wear resistance. These tribological applications usually involve localized mechanical loading but the resulting temperature field can extend much farther. Nevertheless, at locations with zero or negligibly small mechanical loading but with noticeable thermal cycles, the preferential oxidation like in Fig. 1(a) and the subsequent fracture failure are found in these materials. It is well known that chromium oxide is protective and does not lead to localized failure, primarily due to its high Pilling-Bedworth ratio, high strength, and non-porous structure. Indeed in Fig. 1(b) which shows the corresponding isothermal oxidation behavior under the load-free condition, no chromium-oxide fingers are found. The earthworm-like phase is tungsten oxide, below which a tungsten depletion zone is located. The thermodynamics of oxidation cannot distinguish these two sets of experiments in Fig. 1 because the materials and environment in these experiments are the same.

The contrasting behavior of the oxidation experiments in Fig. 1, with details reported in [18–20], is investigated in this paper in Section 2 from the stress induced by concomitant oxidation-diffusion-creep processes as neatly explained in Suo et al. [13], and in Section 3 from the competition between thickening and extending processes of TGO as first discovered by Evans et al. [14,15]. The synopsis of our analysis is given here. *First*, due to the kinematic constraint on material continuity, when the diffusion flux is not divergent-free, a fluid has to change its density, but a solid has to deform whereas a rate-dependent flow sets the stress needed to counterbalance the divergence of the diffusion flux and the elastic deformation sets a time scale to reach this steady state. The mathematical representation is based on the work in Suo [21], termed in this paper as the Stokes-Herring-Suo formalism. Overall speaking, the oxidation process on the oxide-alloy interface requires the mass transport of chromium atoms, and the resulting diffusion flux of chromium atoms is uniaxial and thus not divergent-free. The volumetric strain rate caused by diffusion has to balance with the deviatoric strain rate, i.e., creep driven by lateral stress. *Second*, for a test oxide finger as in Fig. 1(a), results from the Evans model [14,15] suggest that an elastically deforming oxide will progressively and cyclically elongate into the depth direction, while a plastically deforming oxide will redistribute the material addition (due to the Pilling-Bedworth ratio being larger than unity) by plastic flow, leading to thickening in lateral direction, but not extending in depth direction, of the oxide finger. Whether the oxide finger deforms elastically or not relies on the magnitude of oxidation stress and the time needed to establish the steady state. The synergy of the oxidation stress model from Stokes-Herring-Suo formalism and the growth-mode analysis of oxide finger from Evans model leads to a mechanistic interpretation of the mysterious failure in Fig. 1(a) under repeated thermal shocks but no failure in Fig. 1(b) under isothermal condition. In the end, a summary of this work, together with its peculiarities and generalities, will be presented in Section 4.

## 2. Stress induced by concomitant oxidation-diffusion-creep processes

As shown by the problem formulation in Fig. 2, the substrate superalloy initially occupies the half space of $x_3 \leq 0$. Following the notation in [13], the oxide layer thickness is denoted as $h(t)$, and the oxide-substrate interface is located at $x_3 = -s(t)$ as time elapses. For

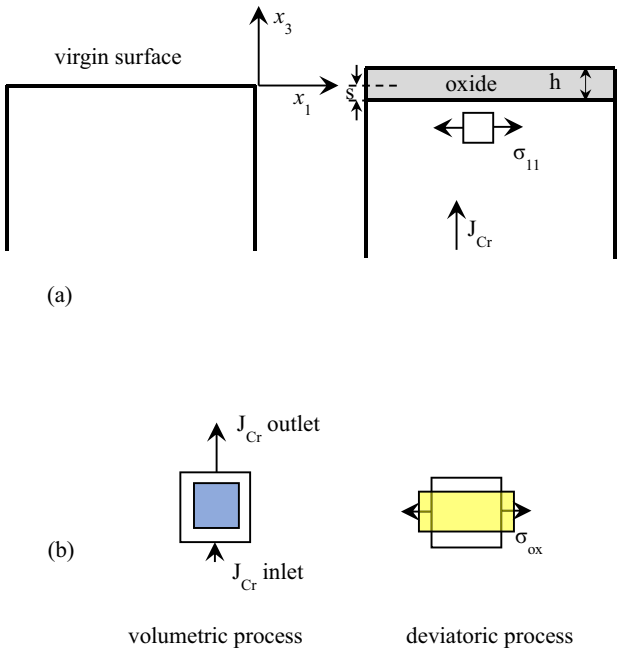


**Fig. 2.** Stress generation from concomitant oxidation-diffusion-creep processes. (a) Schematic illustration of the boundary value problem, notations, and coordinates. (b) Chromium diffusion flux is uniaxial and has a gradient in the depth direction, so that it is not divergent free and a volumetric shrinkage occurs. Creep deformation is a deviatoric process; a lateral expansion is accompanied with a vertical shrinkage.

chromium oxidation, oxygen anions diffuse from outside to the oxide-substrate interface. This process and the interfacial reaction are much faster than chromium diffusion in the substrate superalloy from $x_3 = -\infty$ to $x_3 = -s$, so that the diffusion flux of chromium, $J_{Cr}$, is the rate limiting process. The two length scales, $h$ and $s$, are related by

$$\dot{h}/\dot{s} = \Omega_{ox}/\Omega = \lambda_{PB}, \tag{1}$$

where $\Omega$ and $\Omega_{ox}$ are the atomic volumes of superalloy and oxide, respectively, and $\lambda_{PB}$ is the Pilling-Bedworth ratio (about 2.07 here).

The material extends to infinity in $x_1$ and $x_2$ directions, so that the problem becomes one dimensional in space. The material is free of external load, but it is not necessarily stress free. The stress tensor is biaxial, given by

$$\sigma_{11} = \sigma_{22} = \sigma_{ox}(x_3, t), \sigma_{33} = 0, \tag{2}$$

the mean stress is $\sigma_{mean} = \frac{2}{3}\sigma_{ox}$, and the deviatoric stress is

$$\mathbf{s} = \frac{1}{3}\sigma_{ox}\begin{bmatrix} 1 & & \\ & 1 & \\ & & -2 \end{bmatrix}. \tag{3}$$

Throughout this paper, Latin subscripts run from 1 to 3, and summation convention is implied for repeated indices. As will be shown shortly, a biaxial tensile stress will be generated during oxidation, i.e., $\sigma_{ox} > 0$.

For our creeping solid, the uniaxial constitutive law is represented by a power law,

$$\dot{\varepsilon}^{creep}_{uniaxial} = B\sigma^n_{uniaxial} = \frac{A}{k_B T}\exp\left(-\frac{Q_{creep}}{RT}\right)\sigma^n_{uniaxial}, \tag{4}$$

with the stress exponent $n$ and the pre-factor $B$. The latter has the usual temperature dependence where $Q_{creep}$ is the activation energy, $k_B$ is the Boltzmann constant, $T$ is the absolute temperature, and $R$ is the gas constant. The multiaxial generalization of Eq. (4) is

$$\dot{\varepsilon}^{creep}_{ij} = B\sigma^n_e\frac{3}{2}\frac{s_{ij}}{\sigma_e} = \frac{1}{2\eta}s_{ij}, \tag{5}$$

where $\sigma_e$ is the Mises stress and $\eta$ is the (dynamic) viscosity. The last term is the representation of Stokes creep, regardless of whether the material is Newtonian viscous or not. As shown in Fig. (b), the creep deformation is a deviatoric process, so that the lateral expansion ($\dot{\varepsilon}^{creep}_{11} = \dot{\varepsilon}^{creep}_{2} > 0$) is accompanied with a vertical shrinkage ($\dot{\varepsilon}^{creep}_{33} < 0$).

The strain rate, $\dot{\varepsilon}_{ij}$, relates to the velocity field, $v_i$, by

$$\dot{\varepsilon}_{ij} = \frac{1}{2}(v_{i,j} + v_{j,i}) = \dot{\varepsilon}^{elastic}_{ij} + \dot{\varepsilon}^{creep}_{ij} + \dot{\varepsilon}^{diffusion}_{ij}, \tag{6}$$

whereas $v_{i,j} = \partial v_i/\partial x_j$. From the generalized Hooke's law,

$$\dot{\varepsilon}^{elastic}_{ij} = \frac{1+\nu}{E}\left(\dot{\sigma}_{ij} - \frac{\nu}{1+\nu}\dot{\sigma}_{kk}\delta_{ij}\right), \tag{7}$$

with $E$ being the Young's modulus, $\nu$ Poisson's ratio, and $\delta_{ij}$ the Kronecker delta. The creep rate is given in Eq. (5). The diffusion-induced strain rate, $\dot{\varepsilon}^{diffusion}_{ij}$, arises from a kinematic constraint. For a solid,

$$\nabla\cdot\left(\mathbf{J} + \frac{1}{\Omega}\mathbf{v}\right) = 0, \tag{8}$$

so that a diffusion flux with a nontrivial divergence will lead to a volumetric expansion or shrinkage. Following the isotropic placement rule in Suo [21],

$$\dot{\varepsilon}^{diffusion}_{ij} = -\frac{1}{3}\Omega\delta_{ij}(\nabla\cdot\mathbf{J}). \tag{9}$$

Referring to Fig. 2(b), the diffusion flux of chromium atoms is uniaxial and increases as $x_3$ approaches the oxide-alloy interface from the negative infinity. Thus $\nabla\cdot\mathbf{J} = dJ_{Cr}/dx_3 > 0$, and the corresponding volumetric strain rate in Eq. (9) is negative.

Even with the kinematic relationship in Eq. (9) and the material constitutive law in Eq. (5), the missing link exists for the diffusion flux and the stress should be connected. As the diffusion flux is driven by the gradient of chemical potential and the chemical potential is modified by the mean stress in the bulk (as opposed to the normal stress along the grain boundary), the Herring diffusion [22] is given by

$$\mathbf{J} = -\frac{D}{\Omega k_B T}\nabla\mu = \frac{D}{k_B T}\nabla\sigma_{mean}, \tag{10}$$

where the self-diffusivity $D$ has the usual temperature dependence,

$$D = D_0\exp\left(-\frac{Q_d}{RT}\right). \tag{11}$$

Summarizing the above formulations, we note that Suo [21] unified the viscous flow (or Stokes creep) in Eq. (5) and the Herring diffusion in Eq. (10) through a kinematic rule in Eq. (9), thus denoted hereby as the Stokes-Herring-Suo formalism. In our problem in Fig. 2 (a), $\dot{\varepsilon}_{11} = \dot{\varepsilon}_{22} = 0$, and combining the above equations gives

$$-\frac{2D\Omega}{9k_B T}\frac{\partial^2\sigma_{ox}}{\partial x_3^2} + \frac{1}{2}B\sigma^n_{ox} + \frac{1-\nu}{E}\frac{\partial\sigma_{ox}}{dt} = 0, \tag{12}$$

with the boundary condition of

$$\left.\frac{\partial\sigma_{ox}}{\partial x_3}\right|_{x_3=-s} = \frac{3k_B T}{2D\Omega\lambda_{PB}}\dot{h}. \tag{13}$$

Define the following reference stress, length, and time:

$$\sigma_{ref} = \frac{3k_B T}{2\Omega}, L_{ref} = \sqrt{\frac{2D}{3B\sigma^n_{ref}}}, t_{ref} = \frac{6(1-\nu)}{E}\cdot\frac{1}{3B\sigma^{n-1}_{ref}}. \tag{14}$$

Clearly the length scale results from the comparison between diffusivity and viscosity (both of which are bulk processes here), as similarly defined in Needleman and Rice [23] from the competition between grain-boundary diffusion and grain-interior creep. Normalizing the boundary condition in Eq. (13),

$$\left.\frac{\partial(\sigma_{ox}/\sigma_{ref})}{\partial(x_3/L_{ref})}\right|_{x_3=-s} = \frac{E}{3(1-\nu)\lambda_{PB}\sigma_{ref}}\frac{d(h/L_{ref})}{d(t/t_{ref})} = C_0. \tag{15}$$

To calculate these dimensionless parameters in Eqs. (14) and (15), we need to know the creep properties in Eq. (4) and the lattice diffusivity in Eq. (11), which are assembled in Table 1 according to our prior experimental results in [18–20] and literature data in [11,12,24–26]. As the pre-factor $B$ has an uncertainty of several orders of magnitude, we need to assess the reference time by rewriting Eq. (14) into

$$t_{ref} = \frac{6(1-\nu)}{E}\cdot\frac{L^2_{ref}\sigma_{ref}}{2D}. \tag{16}$$

**Table 1**
Material parameters used in our analysis according to our prior experimental investigations [18–20] and literature data [11,12,24–26].

| Parameter | Value |
|---|---|
| Atomic volume, $\Omega$ | $1.2\times10^{-29}$ m$^3$ |
| Stress exponent in 800–1000 °C, $n$ | ~4.0 |
| Activation energy for creep, $Q_{creep}$ | ~487 kJ/mol |
| Pre-factor for creep, $B$ (at a given temperature) | Varying by many orders of magnitude |
| Activation energy for self-diffusion, $Q_dQ_d$ | 266.1 kJ/mol |
| Pre-factor for self-diffusion, $D_0$ | 44.3 mm$^2$/s |
| Modulus of the oxide, $E_{inclusion}$ | 245 GPa |
| Modulus of the matrix, $E_{matrix}$ | 230 GPa |
| Yield strength of the oxide, $\sigma_Y$ | 1.57 GPa |

For the isothermal oxidation experiment, Fig. 1(b) suggests $L_{ref} \approx 10\ \mu$m, as it has already reached the steady state. From Table 1, at $T$ = 1000 °C, we obtain $\sigma_{ref}$=2.31 GPa and $D$=5.34 × $10^{-16}$ m$^2$/s, leading to a reference time of $t_{ref} \approx 1.7$ h. Experimental findings in [18–20] suggested a growth rate of $\dot{h} \approx 2 \times 10^{-11}$ m/s for this isothermal oxidation condition. Consequently, the above creep, diffusion, and growth parameters lead to a dimensionless parameter $C_0$ of about 0.18.

The partial differential equation in Eq. (12) can be easily solved with results given in Fig. 3. Even with two widely different boundary values, it is found that the steady-state stress field is developed within $t_{ref}$ and over a depth range of $L_{ref}$. For $C_0 \approx 0.18$, an oxidation

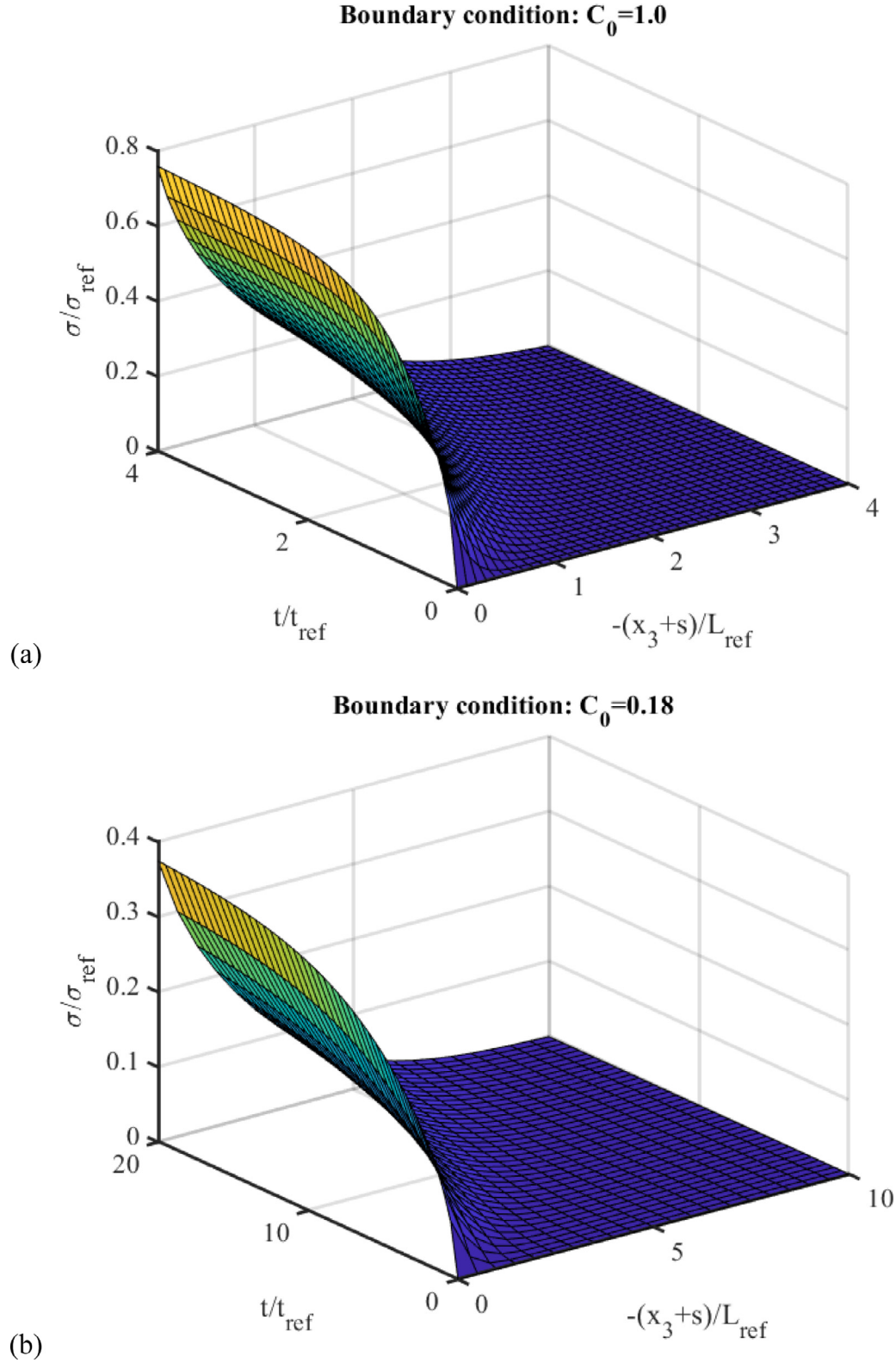


**Fig. 3.** The spatiotemporal evolution of the oxidation stress with two representative values of the normalized boundary condition, $C_0$ in Eq. (15). An oxidation stress of the magnitude of $\sigma_{ref}$ is developed over a depth range of $L_{ref}$ within a time period of $t_{ref}$. These reference parameters are defined in Eqs. (14) and (16).

stress on the order of about 700 MPa will be developed over a depth of about 10 $\mu$m within a few hours. This is certainly achievable as Fig. 1(b) for the isothermal oxidation condition is taken at 200 h. In contrast, experiments in Fig. 1(a) only prescribe a hold time of 15 min, so that it is expected that the oxidation stress will be very low correspondingly and never reaches the steady state. Such a difference will be further elaborated in Fig. 6.

## 3. Thickening versus elongation of oxide fingers

To resolve the contrasting behavior in Fig. 1(a) and (b), we consider the boundary value problem in Fig. 4(a). An elastic-perfectly-plastic oxide finger with yield strength $\sigma_Y$ is embedded within a power-law creeping substrate, subjected to a faraway radial stress over a length of $L$. Studies in Section 2 set the bound of this applied stress. The oxidation process for this axisymmetric finger is simplified by a volumetric growth strain rate of $\dot{\varepsilon}_{growth}$, i.e., the oxide finger simply expands with an isotropic strain of $\dot{\varepsilon}_{growth}t$ when it is free of geometric constraint and internal stress. Define the following two dimensionless parameters:

$$\vartheta_{lateral} = \frac{\dot{r}}{L\dot{\varepsilon}_{growth}}, \vartheta_{vertical} = \frac{\dot{l}}{L\dot{\varepsilon}_{growth}}, \tag{17}$$

which describe the lateral thickening rate and the depth elongation rate, respectively. He and Evans [15] suggests that the oxide finger tends to elongate in the depth direction if it deforms elastically (i.e., $\vartheta_{vertical} > > \vartheta_{lateral}$), while it tends to thicken/expand laterally if it deforms plastically (i.e., $\vartheta_{vertical}$ is comparable to, or smaller than, $\vartheta_{lateral}$).

With the setup in Fig. 4(a), how $\vartheta_{lateral}$ and $\vartheta_{vertical}$ critically depend on the deformation characteristics of the oxide finger is examined here in our boundary value problem through a parametric study. Based on experiments in Fig. 1 and our previous characterizations [18–20], we choose the following dimensionless parameters: $E_{oxide}/E_{alloy}$=1.065, $\nu_{oxide} = \nu_{alloy}$=0.3, $E_{oxide}/\sigma_Y$=156, $r/L = 1/40$, and

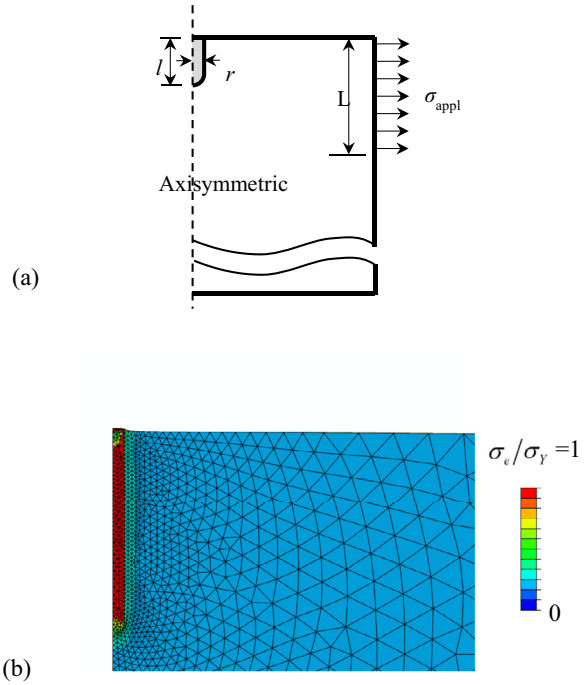


**Fig. 4.** (a) Boundary value problem to examine the growth behavior of an oxide finger into a superalloy substrate. (b) Contour plot of $\sigma_e/\sigma_Y$ at $tB\sigma_Y^n$=1 with $\sigma_{appl}/\sigma_Y$=0.2, $l/L$=0.5, and $\dot{\varepsilon}_{growth}/B\sigma_Y^n$=0.01, when the oxide finger just enters into the plastic deformation.

$n$=4. Thus our results will be represented against the following dimensionless variables:

$$\frac{\sigma_{appl}}{\sigma_Y}, \frac{l}{L}, \frac{\dot{\varepsilon}_{growth}}{B\sigma_Y^n}, tB\sigma_Y^n. \tag{18}$$

The boundary value problem in Fig. 4(a) is modeled in the commercial finite element software, ABAQUS, with a typical mesh shown in Fig. 4(b). The growth strain rate is mimicked by a gradual thermal expansion. As a representative case, we choose $\sigma_{appl}/\sigma_Y$=0.2, $l/L$=0.5, and $\dot{\varepsilon}_{growth}/B\sigma_Y^n$=0.01, and contours of the normalized Mises stress, $\sigma_e/\sigma_Y$, are plotted in Fig. 4(b) at $tB\sigma_Y^n$=1, which roughly corresponds to the onset of yield in the oxide finger.

Provided with a slow oxidation rate (low $\dot{\varepsilon}_{growth}/B\sigma_Y^n$), a low oxidation stress (low $\sigma_{appl}/\sigma_Y$), and a finger of low aspect ratio (low $l/L$), the deformation behavior in the oxide finger tends to be elastic. In other words, short fingers deform elastically as representatively shown in Fig. 5(a). The role of aspect ratio $l/r$ can be understood from the shear-lag model. As shown by Fig. 2(b), the deviatoric creep process leads to a vertical shrinkage of the alloy, which thus applies shear tractions along the vertical interface between finger and alloy. The shear-lag model gives a force balance between $\sigma_{zz}\pi r^2$ and $\sigma_{rz}2\pi rl$, thus leading to $\sigma_{zz} > > \sigma_{rz}$ if the aspect ratio $l/r > > 1$. Then it is more likely for the long fingers to deform plastically. The finger thickening and elongation rates are presented in Fig. 5(b) for a representative case that experiences the elastic-plastic transition as time elapses. Indeed, $\vartheta_{vertical} > > \vartheta_{lateral}$ in the early stage when the oxide finger deforms elastically, but their difference decreases as the deformation transitions into a plastic one.

Experiments in Fig. 1(a) and (b) can now be understood from the stress generation in Fig. 2 and the oxide growth in Fig. 4 as below. *First*, under the isothermal oxidation condition, there is a sufficient time for the steady state to be reached. Recall our estimates of about 700 MPa stress to be developed within hours for chromium oxidation at 1000 °C, which are certainly attainable in Fig. 1(b). If the oxide scale is perturbed and a finger-like protrusion is attempted, the internal stress induced by concomitant oxidation-diffusion-creep processes is high enough to yield this oxide finger, which subsequently prefers to thicken rather than to elongate. The finger-like perturbation will then be suppressed, as shown schematically in the top two rows in Fig. 6. In other words, a continuous oxide layer will form under the isothermal condition. *Second*, the oxidation behavior under repeated thermal shocks in Fig. 1(a) has a very short hold period (being 15 min at 800 °C), which is significantly less than the time scale in Eq. (16) for the internal stress to be fully developed. Thus, a finger-like protrusion deforms elastically (because of the low oxidation stress) and then prefers to elongate rather than to thicken, as shown schematically in the bottom two rows in Fig. 6. This scenario becomes a failure mechanism under thermal fatigue.

Several subtleties need particular attentions for the above rationalization of Fig. 6. The temperature pattern in Fig. 1(a) has a heating stage of 1–3 min (from RT to 800 °C), which is too short compared to the hold period, so that our schematic drawing in Fig. 6 (central row, blue dashed curve) does not differentiate it from the early stage of hold period. The cooling rate is significantly higher, as the samples were quenched in water. The sudden drop of the oxidation stress can be understood from our governing boundary/initial value problem in Eqs. (12) and (13). Upon being quickly cooled to RT, oxidation ceases, and creep and diffusion are essentially non-operating. As there is no diffusion of Cr, there is no need for the balance in Fig. 2(b), and the stress is not needed either. In other words, $\sigma_{ox}(x_3, t)$ accompanies with diffusion and oxidation, and thus clearly vanishes accordingly at room temperature. Lastly, it should be pointed out that earthworm-like oxides in Fig. 1(b) are tungsten oxide, as proved from EDS analysis [20] and the appearance of a tungsten-depleted zone. They are not the chromium-oxide fingers in our analysis.

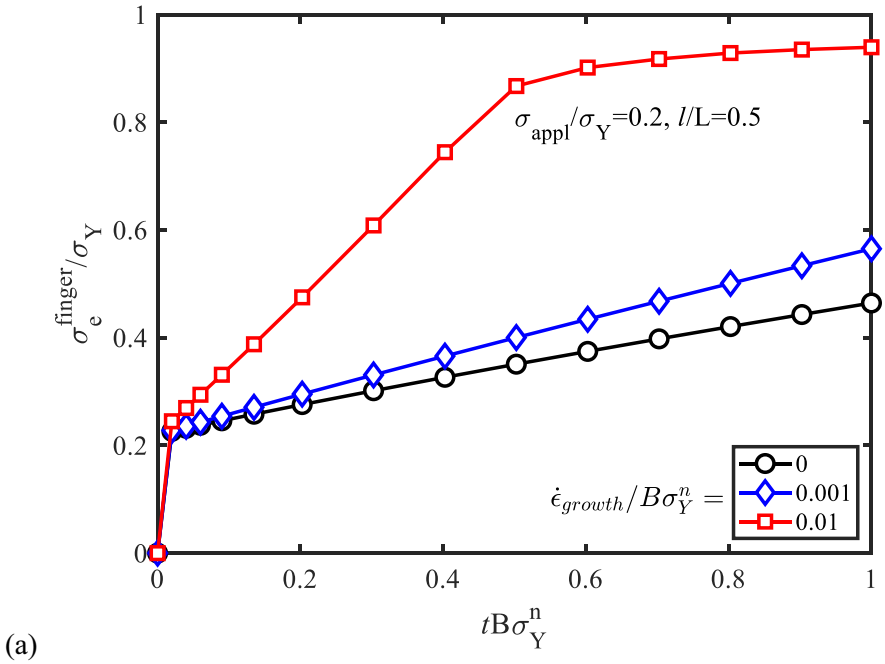


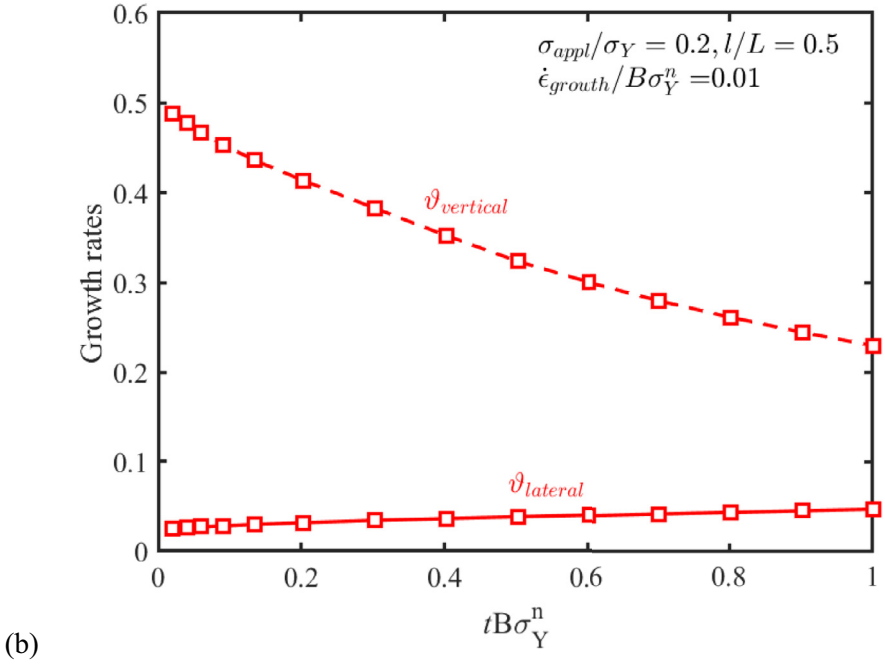


**Fig. 5.** (a) The evolution of the average Mises stress in the oxide finger with respect tot several representative values of $\dot{\epsilon}_{growth}/B\sigma_Y^n$. (b) The elongation rate, $\vartheta_{vertical}$, and the thickening rate, $\vartheta_{lateral}$, as defined in Eq. (17) are shown here for a representative case that experiences a transition from elastic to plastic deformation.

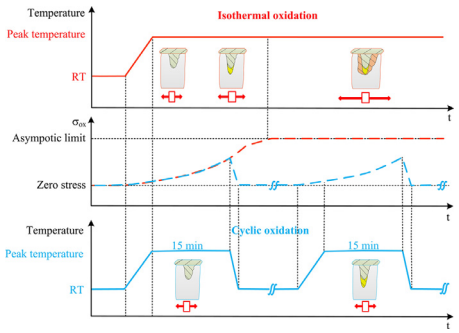


**Fig. 6.** A summary plot that explains the contrasting behavior of cyclic thermal fatigue and isothermal oxidation in Fig. 1(a) and (b), respectively.

## 4. Concluding remarks

As the service conditions of high temperature superalloys are extended to higher temperature, more corrosive environment, and more complex loading patterns, we are confronted with many unprecedented failure modes under these creep-fatigue-oxidation conditions. The Stokes-Herring-Suo formalism has been found to be successful in understanding the stress generation near the thermally grown oxide in the thermal barrier coating system [13]. The same framework is employed in this work to understand the stress generation under concomitant oxidation-diffusion-creep processes with a constant or cyclically varying temperature history. For Co-based superalloys without external load, the oxidation stress can be developed into a sufficiently high value under isothermal condition, which

suppresses the elongation of oxide fingers. On the contrary, thermal shocks are prescribed with a much shorter hold time, so that the steady-state oxidation stress field cannot be realized in time and the resulting elastically deforming oxide fingers prefer to elongate than thicken. While further detailed experimental analyses must be performed, such as the determination of creep parameters, the measurement of elemental distribution, and decoupling the synergy of chromium and tungsten oxidation processes, the essential ideas of stress generation and finger growth should nevertheless find a much wider applicability, particularly for the low-cycle thermal fatigue problems under oxidation conditions.

## Declaration of Competing Interest

The authors declare no competing interests.

## Acknowledgments

This work was supported by the National Natural Science Foundation of China (Nos. 51761027 and 51675255) for the work performed at Lanzhou University of Technology (LUT), by a study-abroad scholarship for outstanding students from LUT to JXW for a one-year visit at University of Tennessee, and by the US National Science Foundation under DMR-1809640 for YFG.

## Supplementary materials

Supplementary material associated with this article can be found in the online version at doi:10.1016/j.actamat.2020.05.002.

## References

[1] J.C. Williams, E.A. Starke Jr, Progress in structural materials for aerospace systems, Acta Mater. 51 (2003) 5775–5799.
[2] R.C. Reed, The Superalloys: Fundamentals and Applications, Cambridge University Press, 2006.
[3] A. Suzuki, T.M. Pollock, High-temperature strength and deformation of $\gamma/\gamma'$ two-phase Co-Al-W base alloys, Acta Mater. 56 (2008) 1288–1297.
[4] A.G. Evans, M.Y. He, J.W. Hutchinson, Mechanics-based scaling laws for the durability of thermal barrier coatings, Prog. Mater. Sci. 46 (2001) 249–271.
[5] D.R. Clarke, C.G. Levi, Materials design for the next generation thermal barrier coatings, Annu. Rev. Mater. Res. 33 (2003) 383–417.
[6] T.L. Sham, S.J. Zinkle, Creep and fatigue issues for structural materials in demonstration fusion energy systems, Trans. Indian Inst. Met. 63 (2010) 331–337.
[7] T.C. Totemeier, H. Tian, Creep-fatigue-environment interactions in INCONEL 617, Mater. Sci. Eng. A 468–470 (2007) 81–87.
[8] C. Pu, Y.F. Gao, Y.L. Wang, T.L. Sham, Diffusion-coupled cohesive interface simulations of stress corrosion intergranular cracking in polycrystalline materials, Acta Mater. 136 (2017) 21–31.
[9] J.F. Wen, Y. Liu, A. Srivastava, A.A. Benzerga, S.T. Tu, A. Needleman, Environmentally enhanced creep crack growth by grain boundary cavitation under cyclic loading, Acta Mater. 153 (2018) 136–146.
[10] W. Niu, Z. Li, F. Ernst, Z. Ren, C. Ye, R.S. Lillard, Stress corrosion cracking of surface-engineered alloys in a simulated boiling-water reactor environment, Corrosion 74 (2018) 635–653.
[11] W. Zhang, X. Wang, Y.Y. Wang, X.H. Yu, Y.F. Gao, Z.L. Feng, Type IV failure in weldment of creep resistant ferritic alloys: I. Micromechanical origin of creep strain localization in the heat affected zone, J. Mech. Phys. Solids 134 (2020) 103774.
[12] W. Zhang, X. Wang, Y.Y. Wang, X.H. Yu, Y.F. Gao, Z.L. Feng, Type IV failure in weldment of creep resistant ferritic alloys: II. Creep fracture and lifetime prediction, J. Mech. Phys. Solids 134 (2020) 103775.
[13] Z. Suo, D.V. Kubair, A.G. Evans, D.R. Clarke, V.K. Tolpygo, Stress induced in alloys by selective oxidation, Acta Mater. 51 (2003) 959–974.
[14] A.G. Evans, M.Y. He, A. Suzuki, M. Gigliotti, B. Hazel, T.M. Pollock, A mechanism governing oxidation-assisted low-cycle fatigue of superalloys, Acta Mater. 57 (2009) 2969–2983.
[15] M.Y. He, A.G. Evans, A model for oxidation-assisted low cycle fatigue of superalloys, Acta Mater. 58 (2010) 583–591.
[16] S. Perusin, B. Viguier, D. Monceau, L. Ressier, E. Andrieu, Injection of vacancies at metal grain boundaries during the oxidation of nickel, Acta Mater. 52 (2004) 5375–5380.
[17] L. Zhu, C. Wei, L. Jiang, Z. Jin, J.C. Zhao, Experimental determination of the phase diagrams of the Co-Ni-X (X=W, Mo, Nb, Ta) ternary systems using diffusion multiples, Intermetallics 93 (2018) 20–29.
[18] R. Cao, H.Y. Zhang, G.H. Liu, H.Y. Che, J.H. Chen, Effect of thermal cycle shocking on microstructure and mechanical properties of Stellite 12 (Co-29Cr-2.3C-3W) cobalt based alloy, Mater. Sci. Eng. A 714 (2018) 68–74.
[19] J.X. Wen, H.Y. Che, R. Cao, H. Dong, Y.X. Ye, H.Y. Zhang, J. Brechtl, Y.F. Gao, P.K. Liaw, Evolution of the mechanical properties of a cobalt-based alloy under thermal shocks, Mater. Des. 188 (2020) 108425.
[20] J.X. Wen, R. Cao, H.Y. Che, H. Dong, H.Y. Zhang, Y.F. Gao, P.K. Liaw, The oxidation effect on the cracking behavior of Stellite 12 alloy under thermal shocks, In Review.
[21] Z. Suo, A continuum theory that couples creep and self-diffusion, J. Appl. Mech. 71 (2004) 646–651.
[22] C. Herring, Diffusional viscosity of a polycrystalline solid, J. Appl. Phys. 21 (1950) 437–445.
[23] A. Needleman, J.R. Rice, Plastic creep flow effects in the diffusive cavitation of grain boundaries, Acta Metall. 28 (1980) 1315–1332.
[24] H.J. Frost, M.F. Ashby, Deformation-Mechanism Maps: The Plasticity and Creep of Metals and Ceramics, Pergamon Press, 1982.
[25] T.G. Nieh, J. Wadsworth, O.D. Sherby, Superplasticity in Metals and Ceramics, Cambridge University Press, 1997.
[26] JMatPro®, Practical Software for Materials Properties, Sente Software Ltd (UK).